ELSEVIER

Earth and Planetary Science Letters 126 (1994) 143–159

EPSL

Plate-scale potential-energy distributions and the fragmentation of ageing plates

Mike Sandiford [a], David Coblentz [b]

[a] *Department of Geology, GPO Box 498, University of Adelaide, Adelaide, S.A. 5005, Australia*
[b] *Department of Geosciences, University of Arizona, Tucson, AZ, USA*

Received 15 November 1993; revision accepted 2 June 1994

Abstract

Geoid anomalies associated with mid-ocean ridge systems and a number of continental margins imply that, on the scale of individual plates, the old ocean lithosphere represents a gravitational potential energy sink. Since lateral variations in potential energy contribute to deviatoric stresses in the lithosphere, the changing potential-energy distributions in individual plates associated with the growth and ageing of the oceanic lithosphere may be expected to result in changes in the intraplate stress field. Analytical models for simple plate geometries using lithospheric density models consistent with small positive (+6 m) geoid anomalies across continental margins show that the growth of oceanic lithosphere over a period of 200 Ma may contribute to a decline in the mean plate potential energy $\overline{U}_p$ of about -1×10^{12} N m^{-1} and thus contribute a mean extensional stress difference $(\overline{\sigma_{zz}}-\overline{\sigma_{xx}})$ in continental lithosphere of up to about 8 MPa (averaged over a 125 km thick lithosphere). These estimates are sensitive to the assumed mean continental potential energy $\overline{U}_c$, about which there is some uncertainty. For higher $\overline{U}_c$, approaching that of the mid-ocean ridges (U_{MOR}), the net decline in $\overline{U}_p$ may be as much as -1.7×10^{12} N m^{-1}, whereas for significantly lower $\overline{U}_c$, approaching that of old ocean lithosphere, plate growth may increase $\overline{U}_p$ transiently by up to 2.7×10^{12} N m^{-1}, leading to compression in the continents. In the African and Antarctic plates the ageing of the ocean lithosphere since the late Jurassic is estimated to have contributed to a decline in $\overline{U}_p$ of about -0.6×10^{12} and -0.95×10^{12} N m^{-1} respectively, contributing a mean stress difference of about 5 MPa and 7.5 MPa in the respective continents. Whereas the predicted stress changes associated with ageing of the oceanic lithosphere are significantly smaller than most laboratory-based estimates of the extensional strength of the lithosphere, they may provide an important contribution to the stress fields that eventually lead to the fragmentation of ageing plates.

1. Introduction

The origin of the stress fields responsible for continental extension remains controversial [e.g., 1–3], with much of the debate focussing on the relative roles of lithospheric sources associated with distant plate boundary activity (which contributes to so-called *passive* rifting) and the asthenospheric mantle (so-called active rifting). Our purpose here is to consider the role of intraplate sources of stress related to the distribution of

[PT]

SSDI 0012-821X(94)00126-J

gravitational potential energy, U_l, across individual continental plates. Lateral variations in potential energy resulting from density variations in the lithosphere have long been recognized as an important source of intraplate stress and associated deformation [e.g., 4–7]. Because the mean potential energy of a plate, $\overline{U}_p$, depends on the relative amounts of young and old oceanic lithosphere and continental lithosphere, it will vary as the plate ages. The controls on this variation in potential energy with plate ageing forms the main focus of this paper.

In the absence of tractions imposed at plate boundaries or at the base of the plates, the intraplate stress field can be directly related to the plate-scale potential-energy distribution. Following Dahlen [8] we term this state the *ambient state*. In the ambient state, parts of the plate with potential energy in excess of the plate mean $\overline{U}_p$ will, in general, experience deviatoric tension, while parts of the plate with potential energy less than $\overline{U}_p$ will, in general, experience deviatoric compression. The ambient state is particularly relevant to the intraplate stress field in slow-moving plates largely surrounded by mid-ocean ridges, such as the African and Antarctic plates [e.g., 1]. Changes in the mean plate potential energy attendant on the growth of old ocean lithosphere in such plates should therefore correspond to changes in the *ambient* intraplate stress field. In this paper we calculate the potential energy changes accompanying the growth of large plates. Because potential-energy variations correlate with the mass dipole moment of the lithospheric density distribution [6,7], and therefore with the geoid, we can use observed geoid anomalies associated with ocean ridge systems and continental margins as a first-order constraint on the potential-energy distribution within the present-day plates. The focus of this paper is how this potential-energy distribution may evolve with time in such a way as to engender the possibility of extensional failure within continental lithosphere. We test this hypothesis by evaluating the plate-scale evolution of potential energy for a simple circular plate surrounded by an ocean ridge system. We then evaluate the changes in the potential-energy distribution in the African and Antarctic plates since the late Jurassic using the seafloor age data of Royer et al. [9] and show that the ambient tectonic stress state within continental Africa and Antarctica has become increasingly more extensional as the plate has aged, thus potentially contributing to the stress field responsible for the observed continental rifting in these plates. We begin with an assessment of the distribution of lithospheric potential energy at the plate scale.

2. Geoid anomalies and potential-energy variations

Variations in the gravitational potential energy of the lithosphere, ΔU_l, correlate with the dipole moment of the lithospheric density distribution [e.g., 6,7], and therefore can be directly related to the lithospheric component of the observed geoid anomalies ΔN_l [e.g., 10,11]:

$$\Delta U_l = \frac{g^2}{2\pi G}\Delta N_l$$

where g is the gravitational acceleration and G is the gravitational constant (note that the potential energy varies with the geoid anomaly as approximately 0.23×10^{12} N m^{-1} m^{-1}). The main problem with using this relationship is resolving the lithospheric contribution of the geoid anomalies from the much larger amplitude anomalies associated with the dynamic processes of plate tectonics and mantle convection [e.g., 12].

Positive geoid anomalies of up to 10–15 m associated with a number of mid-ocean ridge segments [13–15] (see discussion by Forsyth [16]), as well as age-correlated geoid offsets across fracture zones [17,18], imply that ageing of the ocean lithosphere is accompanied by a decline in potential energy. In a recent summary, Forsyth [16] concluded that the half-space model for the cooling ocean lithosphere provides an adequate approximation for geoid anomalies in ocean lithosphere younger than about 80–100 Ma. The geoid anomaly, expressed relative to the mid-ocean ridge, associated with ageing of the ocean litho-

sphere which is assumed to cool with time, t, as a half-space is given by [e.g., 13]:

$$\Delta N_0 = -\frac{2\pi G\rho_m \alpha T_m \kappa t}{g}\left(1+\frac{2\rho_m \alpha T_m}{\pi(\rho_m-\rho_w)}\right)$$

where T_m is the reference temperature of the mantle, ρ_m and ρ_w are the density of the mantle (at T_m) and water respectively, α is the thermal coefficient of expansion, and κ is the thermal diffusivity. Note that for the cooling half-space model the geoid anomaly is linear in time.

The lithospheric contribution to geoid anomalies in old oceanic lithosphere is poorly constrained. Parsons and Richter [14] showed that there are significant discrepancies between the predictions of the thermal plate and half-space models for lithosphere older than about 40–60 Ma (Fig. 1). In view of the absence of evidence for the very large geoid anomalies in very old ocean lithosphere consistent with a simple linear age relationship, we assume that the old lithosphere is thermally stabilised and model the geoid anomalies in ageing oceanic lithosphere as a bilinear age function with a critical age ($t_c = 84$ Ma) as shown in Fig. 1. Note that this behaviour approximates the geoid anomalies predicted by the thermal plate model [e.g., 14], and has the virtue of admitting very simple analytical expressions for the potential energy evolution for simple plate geometries (see below).

The geoid anomaly predicted for the cooling half-space model (as well as the thermal plate model) is strongly dependent on the thermal parameters, which are the subject of some uncertainty. In the calculations presented below we use a set of thermal parameter values (Table 1) consistent with $d(\Delta N_0)/dt = -0.15$ m/Ma, which compares favourably with the observed geoid anomaly over the Mid-Atlantic Ridge at 44.5°N [13] and elsewhere [15] as well as with the geoid offsets across fracture zones [18]. This parameter set equates with a total geoid anomaly of −12.7

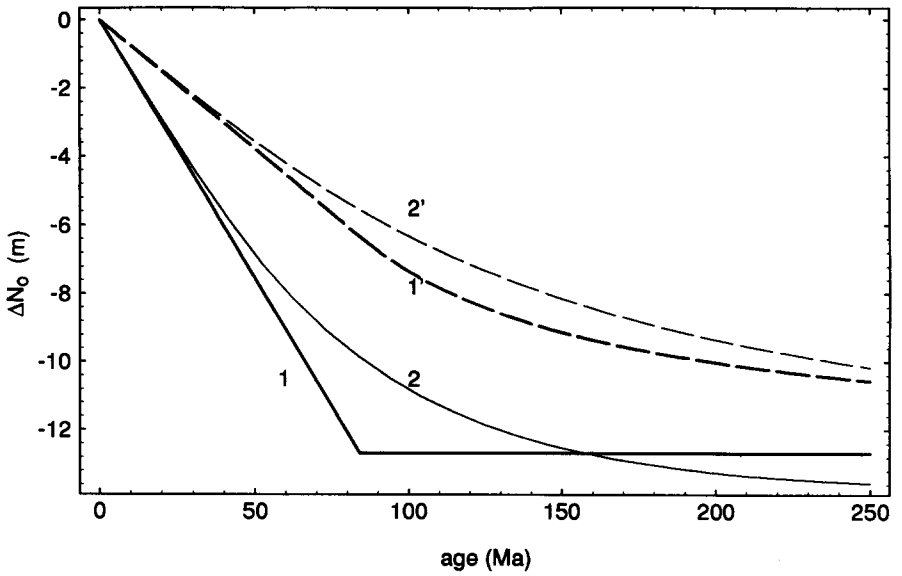

Fig. 1. We assume a bilinear dependence of the geoid anomaly on the age of the ocean lithosphere as illustrated by curve 1. For $t < 84$ Ma the anomaly is given by the half-space model, while for $t > 84$ Ma the anomaly is assumed to be age independent. Using the thermal parameter set in Table 1 the geoid anomaly for the young ocean varies as -0.15 m Ma^{-1}, with a total anomaly of -12.6 m over 84 Ma. For comparison, curve 2 shows the predicted anomaly for the thermal plate model, after Parsons and Richter [14]. Curves 1′ and 2′ show the time evolution of the mean ocean lithosphere geoid anomaly assuming a simple one-dimensional spreading at constant velocity for the models corresponding to curves 1 and 2 respectively. Geoid anomalies are shown relative to ocean lithosphere of age 0 (i.e., relative to the mid-ocean ridge), with corresponding potential-energy anomalies of 0.23×10^{12} N m^{-1} m^{-1}.

Table 1
Values of parameters used in the calculations. The thermal parameter values used here are consistent with geoid anomalies giving $d(\Delta N_0)/dt$ m Ma^{-1} in the ageing ocean lithosphere (see text for discussion)

Parameter	Value
κ	0.87×10^{-6} m^2 s^{-1}
α	3×10^{-5} °K^{-1}
ρ_m	3238 kg m^{-3}
ρ_m	1030 kg m^{-3}
T_m	1280°C
t_c	84 Ma
U_{MOR}	2.391×10^{14} N m^{-1}
g	9.82 m s^{-2}
G	$6.673\ 10^{-11}$ m^3 kg^{-1} s^{-2}

m over 84 Ma with a corresponding reduction in potential energy of -2.9×10^{12} N m^{-1} (which therefore defines an absolute lower limit to the mean plate potential energy relative to the mid-ocean ridges—see Fig. 1). Following [11] we equate the potential energy of the mid-ocean ridge (U_{MOR}) with a column of unit surface area extending to the depth 125 km, with a density structure appropriate to the mid-ocean ridge system. The estimate of 2.391×10^{14} N m^{-1} for U_{MOR} is significantly greater than ocean lithosphere with an age of 84 Ma ($U_0 \mid_{t=84Ma} = 2.362 \times 10^{14}$ N m^{-1}), with the ratio of the potential energy of 84 Ma ocean lithosphere to that of the mid-ocean ridge estimated at approximately 0.988.

In comparison with the mid-ocean ridges, the lithospheric contributions to the geoid anomalies, and hence potential-energy distributions, associated with continental margins and the interior of continents are far less clear. While there are significant spatial variations in the geoid height, and hence the distribution of U_l, within continents, the continental lithsophere is not subject to the systematic temporal changes in U_l of the sort exhibited by the ocean lithosphere. Consequently it suffices for the purposes outlined below to deal only with the mean potential energy of the continents ($\overline{U}_c$). On the basis of averages taken over large areas Turcotte and McAdoo [12] concluded that there was no systematic difference in the geoid height between old ocean basins (older than Cretaceous) and continental masses. Such an interpretation implies that the mean potential energy of the continental lithosphere is equivalent to old ocean basins (i.e., $\overline{U}_c' = 0.988$, where the prime signifies that the relevant potential energy term, in this case the mean of the continental lithosphere, is normalized relative to the potential energy of the mid-ocean ridge, which is $\overline{U}_c' = \overline{U}_c / U_{MOR}$). However, the data show very substantial differences between continents, with the mean geoid of the African continent some 40 m higher than the North American continent and 10 m higher than the mean for the Atlantic and Pacific ocean basins older than Cretaceous. This observed intercontinental variation far exceeds the plausible lithospheric contributions to geoid anomalies and therefore must reflect long-wavelength sublithospheric contributions. Moreover, a number of continental margins are characterized by distinct positive anomalies of the order of 4–6

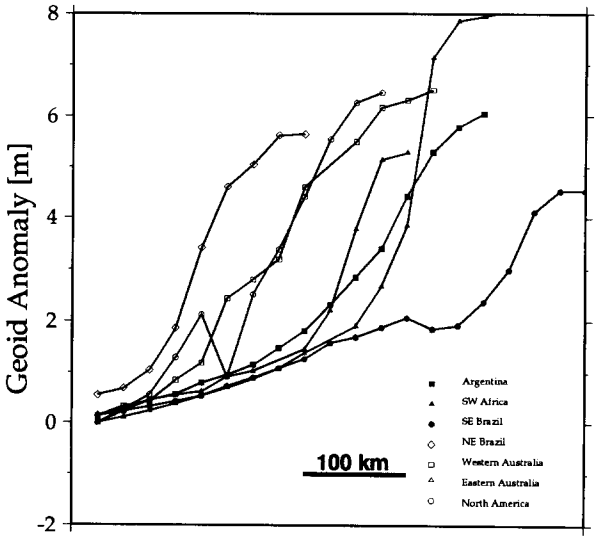

Fig. 2. Observed geoid anomalies (ΔN) across seven passive continental margins. The North American profile is from Haxby and Turcotte [13], the Brazilian profile is from Coblentz and Richardson [27], and the five other margins are from Coblentz et al. [1]. The geoid anomalies have been normalized such that $\Delta N = 0$ corresponds to the oceanic basin with a bathymetry of -4000 m. The transition from ocean to continent is from left to right.

m across the transition from the ocean basin to sea-level on the continental margin [10,11,13] (see Fig. 2), and imply that a continental lithospheric column supporting sea-level elevation has a potential energy equivalent to ocean lithosphere that is about 44 Ma old (i.e., $U_c' \mid_{s=0\,\mathrm{km}} = 0.9936$). (Here, s = elevation of the continental surface relative to sea level.)

Since the lithospheric contribution to the geoid anomaly reflects the dipole moment of the near-surface density distribution, the observed geoid anomalies across continental margins can also be used to constrain the continental lithospheric density structure. Coblentz et al. [11] have shown that a lithospheric thickness of 125 km and a crustal density of 2750 kg/m^3 is consistent with a continental marginal geoid anomaly of +6 m. Moreover, such a density structure is consistent with the interpretation proposed by a number of workers [1,2,19,20] that an isostatically compensated continental lithospheric column supporting about 1 km of surface elevation above sea level is in potential energy balance with the mid-ocean ridges (i.e., $U_c' \mid_{s=1\,\mathrm{km}} = 1$). Whereas the generally poor resolution of the geoid in mountainous regions precludes definitive correlation between topography and potential energy within the continents, some evidence of the correlation is provided by the lithospheric contribution to the geoid anomaly of 24–27 m for the Andean Altiplano inferred by Froidevaux and Isacks [21]. Such inferences are consistent with a geoid that varies with continental topography as 6–7 m km^{-1}, corresponding to a potential energy variation of about 1.3×10^{12} N m^{-1} km^{-1}. For a continent with an average elevation of 500 m, this correlation suggests a mean continental potential energy of $\overline{U_c'} = 0.997$. While in no way validating this estimate, we note that it is consistent with the observed mean geoid over Africa [12].

Our main purpose in the calculations presented in the following sections is to assess time-dependent variations in the potential-energy distribution accompanying plate growth about a continent with a density structure consistent with a positive geoid anomaly of 6 m across the continental margin. For a mean elevation of 500 m, close to the global continental average, the mean potential energy of such a continent is approximately $\overline{U_c'} = 0.997$. However, noting that the available geoid data imply that considerable uncertainty is attached to the potential-energy distribution in the continental lithosphere we also present results for the range of continental lithospheric potential-energy distributions ($\overline{U_c'} =$ 0.988–1.0) corresponding to the full range of potential energies reflected in the ageing ocean lithosphere.

Table 2
Descriptions of parameters used in defining the potential energy of an ageing plate

Parameter	Description
U_l	Potential energy (PE) of local lithospheric column
$\overline{U_p}$	Mean PE of lithospheric plate
$\overline{U_c}$	Mean PE of the continental lithosphere
$\Delta\overline{U_p^c}$	The difference $\overline{U_c}$ - $\overline{U_p}$
	(for the circular plate model this is equivalent to the change in $\overline{U_p}$ with time)
$\overline{U_p'}$	$\overline{U_p}$ normalized relative to MOR (= $\overline{U_p}/U_{MOR}$)
$\overline{U_c'}$	$\overline{U_c}$ normalized relative to MOR (= $\overline{U_c}/U_{MOR}$)
$\overline{U_o}\mid_{t=t_c}$	Mean PE of the ocean lithosphere younger than t_c
v_{sp}	Plate spreading velocity
r_c	Continental radius
v'	Normalized spreading rate (= v_{sp}/r_c)

3. Circular plate model

3.1. Model formulation

Changes in the mean potential energy of an ageing plate surrounded by mid-ocean ridges will reflect a competition between the growth of new seafloor at the ridges, which tends to increase $\overline{U}_p$, and the ageing of existing ocean lithosphere, which tends to decrease $\overline{U}_p$ (Table 2 provides a description of all parameters used below in defining the potential energy of an ageing plate). To demonstrate the importance of ageing of ocean lithosphere on $\overline{U}_p$ we begin by assuming a very simple plate geometry consisting of a circular continent, of radius r_c, surrounded at time $t = 0$ by a system of incipient mid-ocean ridges spreading with a constant velocity v_{sp}. We assume that the mean potential energy of the continental part of the plate, $\overline{U}_c$, is time invariant and, since initially the plate is composed entirely of continent, the mean plate potential energy is initially equal to $\overline{U}_c$. The change in mean plate potential energy with time can therefore be expressed as the difference between the mean continental and the mean plate potential energies which we term $\Delta\overline{U}_p^c (= \overline{U}_c - \overline{U}_p)$, and which is the form used in all the figures.

As the oceanic ridge spreads and the plate ages and grows, the relative percentages of the principal lithospheric types (young oceanic, old oceanic, and continental lithosphere) change. The relative proportion of the lithospheric types making up the total plate area at any time t is given by:

$$A_c = \frac{1}{(v't+1)^2}$$

$$A_{yo}|_{t<t_c} = \frac{(v't+1)^2 - 1}{(v't+1)^2}$$

$$A_{yo}|_{t>t_c} = \frac{(v't+1)^2 - (v'(t-t_c)+1)^2}{(v't+1)^2}$$

$$A_{oo}|_{t<t_c} = 0$$

$$A_{oo}|_{t>t_c} = \frac{(v'(t-t_c)+1)^2 - 1}{(v't+1)^2}$$

where A_c, A_{yo} and A_{oo} are the proportional areas of the continent, young ocean and old ocean respectively, t_c is the age at which old ocean lithosphere starts to form, and v' is the normalized spreading velocity given by the ratio of the spreading velocity to the continental radius ($v' =$

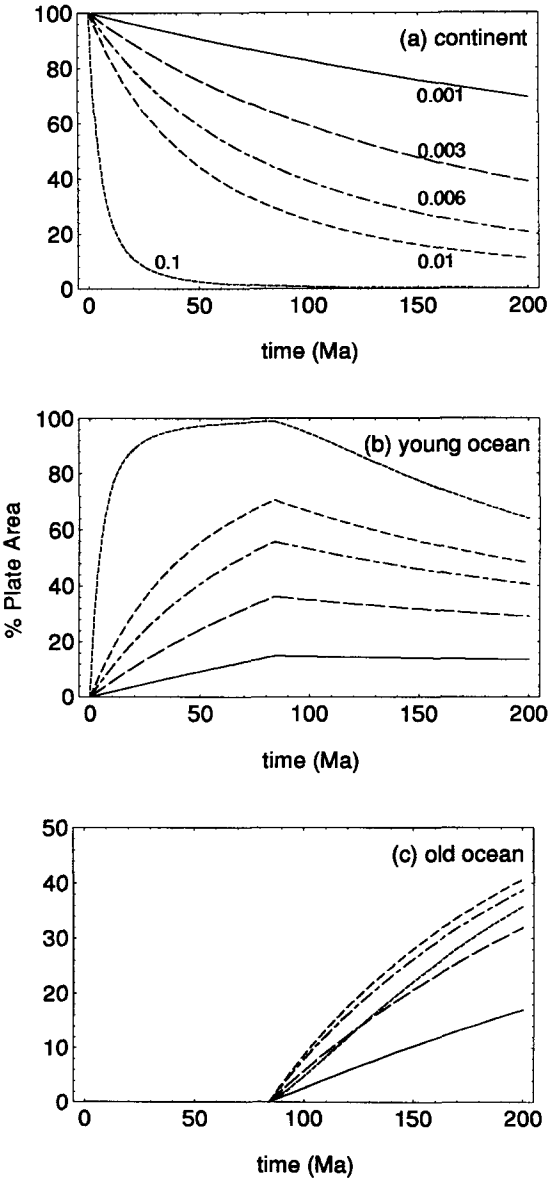

Fig. 3. Percentage areas of the principal lithospheric types for the circular continental plate. Contours are for normalized spreading velocity $v' = 0.001$, 0.003, 0.006, 0.01 and 0.1 Ma^{-1}.

v_{sp}/r_c). Fig. 3 shows the percentage of total plate area of continents, young ocean and old ocean as a function of time for a range of v'. We note that for spreading rates in the range 1–5 cm yr^{-1} and continental radii in the range 500–3000 km the range of v' is 0.003–0.1 Ma^{-1}, with higher spreading velocities and lower continental radii corresponding to higher v'. Fig. 3 shows that for the circular plate model the proportion of continent declines continuously through time as the surrounding ocean grows, while the proportion of young oceanic lithosphere increases rapidly until t_c, and thereafter declines as the proportion of old ocean lithosphere begins to increase.

Assuming the bilinear functional dependence of geoid anomaly on age, as shown in Fig. 1, the difference in potential energy between the mid-ocean ridge and ageing ocean lithosphere ($\Delta U_o^{MOR} = U_{MOR} - U_o|_t$) at any time $t < t_c$ after the onset of spreading is given by:

$$\Delta U_o^{MOR}|_{t<t_c} = -\rho_m \alpha T_m \kappa t g \left(1 + \frac{2\rho_m \alpha T_m}{\pi(\rho_m - \rho_w)}\right)$$

For this simple plate geometry the mean potential energy of the plate relative to the mid-ocean ridge at any time $t < t_c$ is given by:

$$\overline{U}'_p|_{t<t_c} = \frac{\overline{U}'_o|_t\left((v't+1)^2 - 1\right) + \overline{U}'_c}{(v't+1)^2}$$

where $\overline{U}'_o|_t$ is the normalized mean potential energy of the oceanic part of the plate at time t. Since the geoid anomaly is linear in time for young ocean lithosphere, $t < t_c$:

$$\overline{U}'_o|_{t<t_c} = 1 + \frac{\Delta U_o^{MOR}|_t}{2U_{MOR}}\left(\frac{1}{v't+1}\right)$$

Note that the term $(v't+1)^{-1}$ gives the ratio of the circumference of the plate at time $t = 0$ to that at time $t = t$. For $t > t_c$:

$$\overline{U}'_p|_{t>t_c} = \frac{\overline{U}'_o|_{t_c}\left((v't+1)^2 - (v'(t-t_c)+1)^2\right)}{(b't+1)^2} + \frac{\left(1 + \frac{\Delta U_o^{MOR}|_{t=t_c}}{U_{MOR}}\right)\left((v'(t-t_c)+1)^2 - 1\right)}{(v't+1)^2} + \frac{\overline{U}'_c}{(v't+1)^2}$$

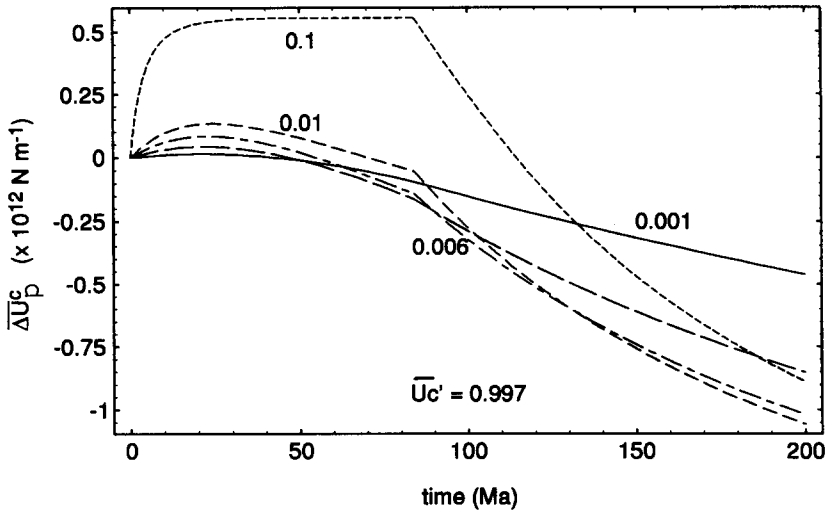

Fig. 4. The change in mean plate potential energy, expressed as ($\Delta\overline{U}^c_p|_t (= \overline{U}_c - \overline{U}_p$, in units of $\times 10^{12}$ N m^{-1}), as a function of time for the ageing circular plate model assuming $\overline{U}'_c = 0.997$ (i.e., for a continent with a mean elevation of 500 m and a density structure appropriate to a geoid anomaly of +6 m across the continental margin). The figure is contoured for normalized spreading rates $v' = 0.001$, 0.003, 0.006, 0.01 and 0.1 Ma^{-1}.

where the first term is the contribution of the young ocean lithosphere, the second term is the contribution of the old ocean lithosphere, and the third term is the contribution of the continental lithosphere. The term $\overline{U}_o' \mid_{t_c}$ gives the mean potential energy of the ocean lithosphere younger than t_c and is given by:

$$\overline{U}_o' \mid_{t_c} = 1 + \frac{\Delta U_o^{MOR} \mid_{t=t_c}}{2U_{MOR}} \left(\frac{v'(t - t_c) + 1}{v't + 1} \right)$$

3.2. Main results

The analysis presented above shows that the time evolution of the potential-energy distribution for this simple circular plate geometry depends on only four parameters: the normalized mean continental potential energy, $\overline{U}_c'$, the ratio of the spreading rate to the continental radius, v', the age at which old ocean lithosphere begins to form, t_c, and the potential energy of the mid-ocean ridge, U_{MOR}. In all the calculations presented here we assume $t_c = 84$ Ma and $U_{MOR} = 2.391 \times 10^{14}$ N m^{-1} (Table 1). The influence of both $\overline{U}_c'$ and v' on the evolution of the mean plate potential energy, expressed as $\Delta\overline{U}_p^c (= \overline{U}_c - \overline{U}_p)$, over a 200 Ma interval is shown in Figs. 4–6. The salient features of the circular plate model results are summarised below:

(1) For our preferred continental density structure with a mean potential energy of $\overline{U}_c' = 0.997$, ocean growth causes a significant long-term decline in the mean plate potential energy (Fig. 4), provided that $v' > 0.005$ (Fig. 6d), with a maximum calculated $\Delta\overline{U}_p^c$ of -1×10^{12} N m^{-1} over 200 Ma. Note that a significant long-term decline in $\overline{U}_p$ is predicted provided $\overline{U}_c' > 0.995$ (Figs. 5c and 6d).

(2) The decline in $\overline{U}_p$ after 200 Ma is greatest for normalized spreading rates in the range $v' = 0.004$–0.02 (as indicated by the minima in the curves in Fig. 6d), reflecting the fact that for high spreading velocities the rapid production of new lithosphere around the circumference of the plate partly ameliorates the effect of ageing of older oceanic lithosphere.

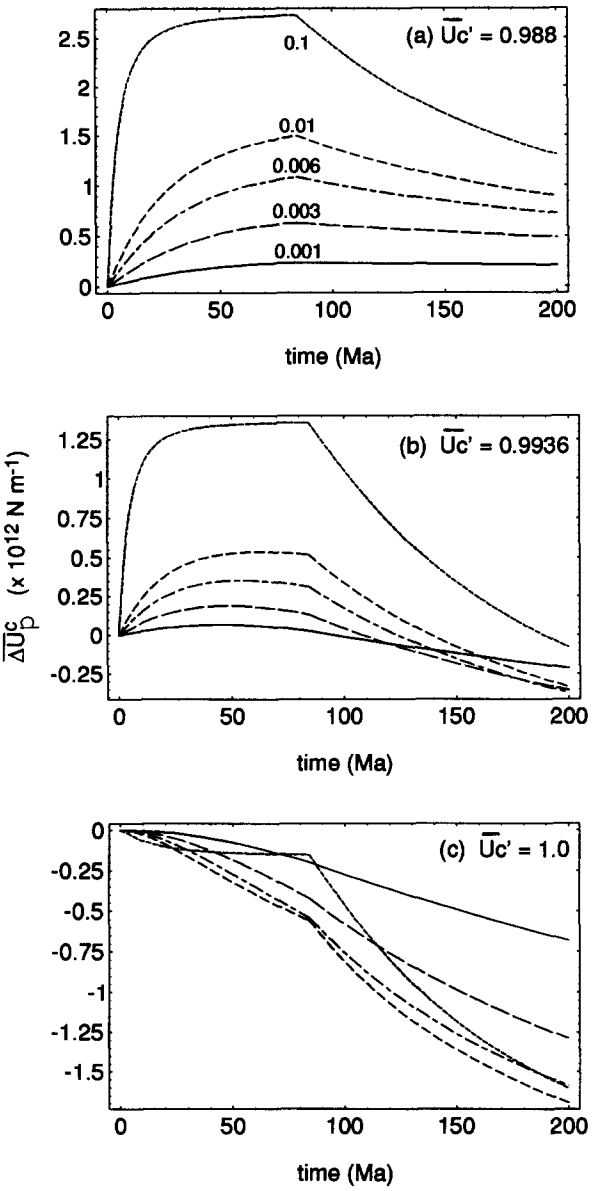

Fig. 5. As for Fig. 3, but showing various $\overline{U}_c'$ (= 0.998, 0.9936 and 1.0) corresponding to the full range of potential energies reflected in the ageing ocean lithosphere.

(3) Transient increases in the mean plate potential energy may be associated with the initial stages of spreading for all initial conditions with $\overline{U}_c' < 1$ (Figs. 4, 5a and 5b). This effect is restricted to times less than t_c and is favoured by high normalized spreading rates (Fig. 6)

and by low $\overline{U}_c'$ (for $v' = 0.1$ Ma^{-1} and $\overline{U}_c' = 0.988$ the calculated transient $\Delta\overline{U}_p^c$ is $+2.7 \times 10^{12}$ N m^{-1} at 84 Ma). Note that such transient increases in potential energy accompanying the initial growth of ocean lithosphere may provide a physical explanation for basin inversion processes.

4. The ageing of the African and Antarctic plates

The preceding discussion implies that the growth and ageing of ocean lithosphere in plates largely surrounded by spreading ridges, such as the African and Antarctic plates, may have important ramifications for the stress regimes in the

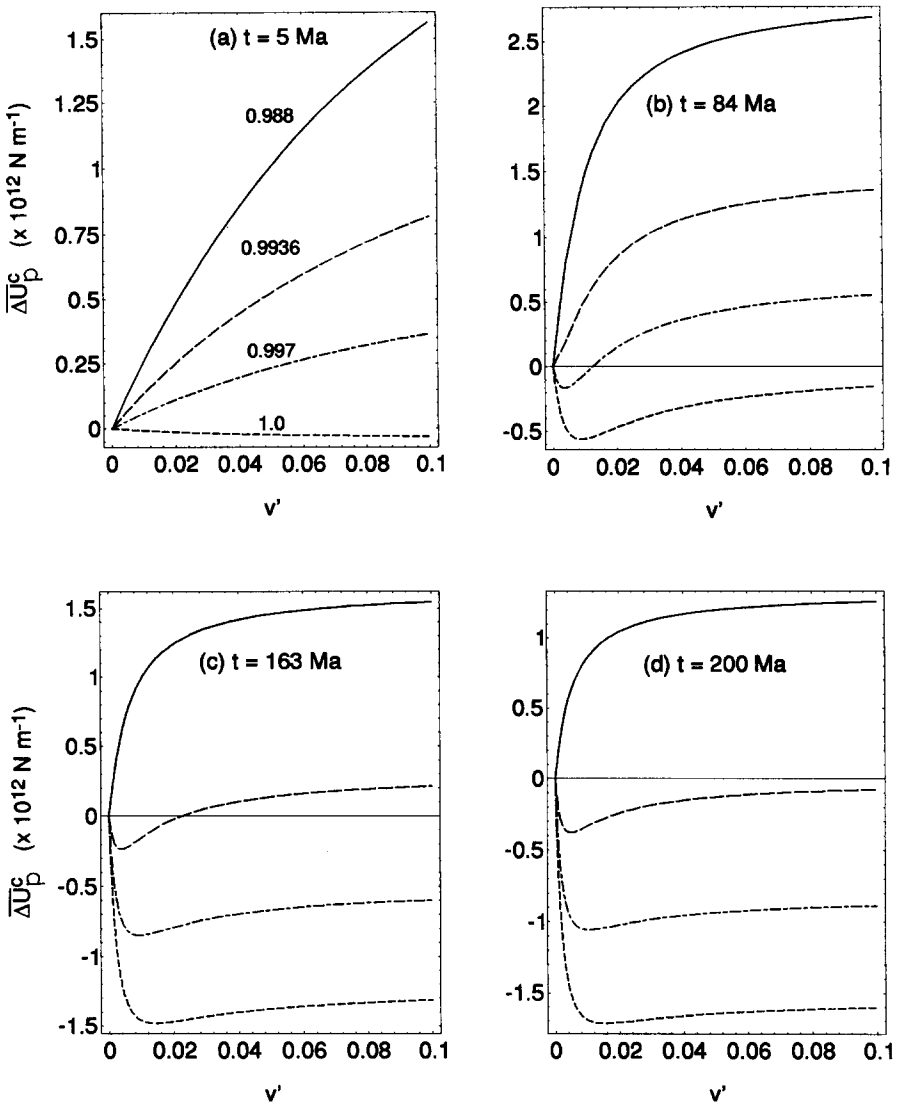

Fig. 6. Illustration of the dependence of the mean plate potential energy, expressed as $\Delta\overline{U}_p^c$ ($= \overline{U}_c - \overline{U}_p$, in units of $\times 10^{12}$ N m^{-1}), on the normalized spreading velocity v' (in units of Ma^{-1}) for given times 5 Ma (a), 84 Ma (b), 163 Ma (c) and 200 Ma (d) after the onset of seafloor spreading for the circular plate model. Contours are for $\overline{U}_c' = 0.988$, 0.9936, 0.997 and 1.0.

continents. Some credence to the efficacy of this process is provided by the fact that both the African and Antarctic plates are experiencing (or in the recent geological past have experienced) extensional failure. In view of the obvious limitations imposed by the highly idealized circular plate model described above, it seems sensible to pursue the ramifications of this idea using more realistic time evolutions for the growth of the ocean lithosphere in these plates. In this section we use the seafloor age data of Royer et al. [9] to assess the changes in the potential energy of the African and Antarctic plates over the last 163 Ma (i.e., since the late Jurassic).

4.1. The African plate

In the calculations summarized here we disregard the changes in plate configuration associated with convergence along the northern boundary with the Eurasian plate, which has undoubtedly resulted in the subduction of some oceanic lithosphere in this time interval. However, plate convergence rates constrained by paleomagnetic data [e.g., 9] imply that the loss of ocean lithosphere through subduction along the northern margin of the African plate has been small compared to the contribution of new oceanic lithosphere through spreading along the Southern At-

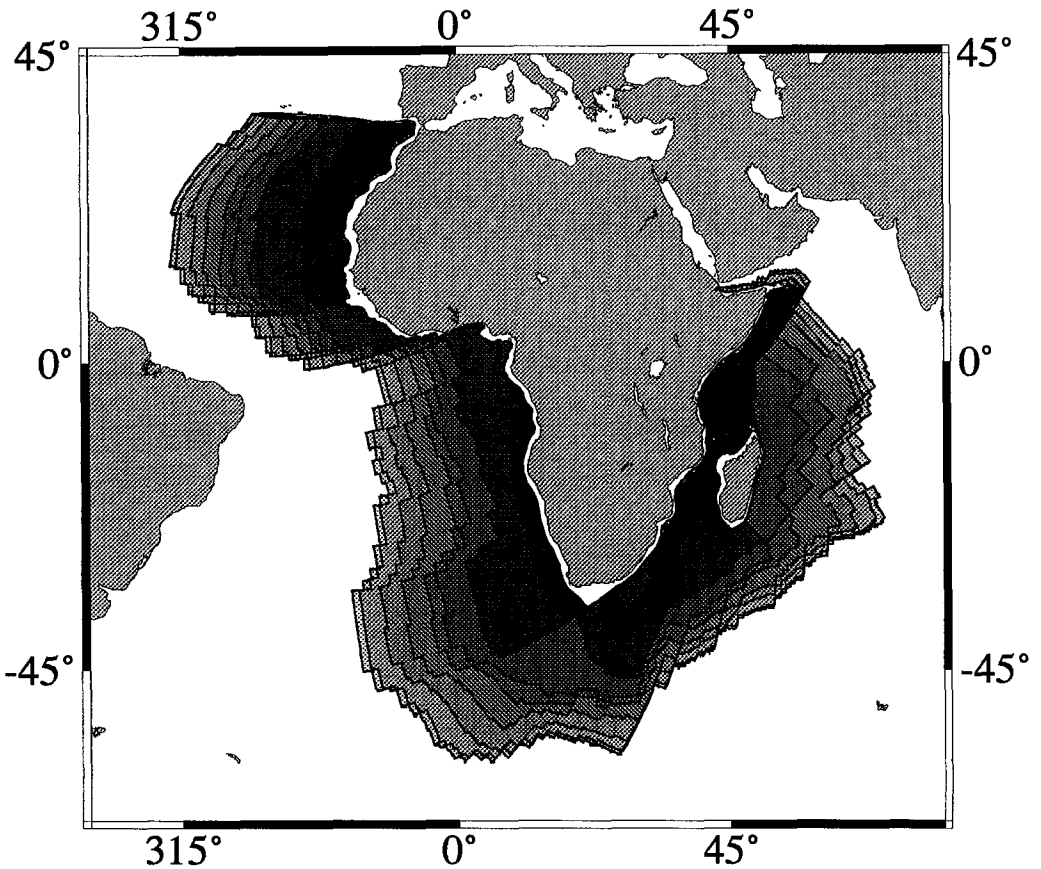

Fig. 7. The area of the African plate over the last 163 Ma. Shaded areas correspond to the area added to the plate during the Pliocene (5.3 Ma), Miocene (23.7 Ma), Oligiocene (36.6 Ma), Eocene (57.8 Ma), Paleocene (66.4 Ma), Late Cretaceous (84 Ma), mid-Cretaceous (119 Ma), Early Cretaceous (144 Ma) and late Jurassic (163 Ma) respectively (see Table 3).

lantic and Indian Ocean ridge segments (the ratio of ocean loss to growth is estimated at about 1:6).

In order to assess the time evolution of $\overline{U}_p$ for the whole African plate we use the estimates of the mean continental potential energy for the African continent as discussed above. The mean elevation of the continent (including the continental margins) is 492 m, and thus a continental density structure appropriate to a continental marginal geoid anomaly of +6 m gives $\overline{U}_c' = 0.997$. There have undoubtedly been some changes in the elevation, and hence potential energy, of parts of the continent since the late Jurassic. However, in the calculations presented below we consider only the contribution of the ageing oceanic lithosphere to the plate-scale potential energy distribution, because as we have shown above (and in contrast to the continental lithosphere) the potential energy of the ageing oceanic lithosphere can be readily approximated on the basis of age.

The growth of the African plate, based on the seafloor age data of Royer et al. [9], is shown in Fig. 7. The relative areas of the regions defined by the magnetic anomalies are listed in Table 3. The cumulative area of the plate is listed in Table 3 and is plotted in Fig. 8a. The plate has grown by 4.31×10^7 km^2 over the last 163 Ma, increasing smoothly with the exception of an anomalously rapid spreading interval between the Oligiocene (36.6 Ma) and the Miocene (23.7 Ma),

Table 3
Area of the African plate

Age	Ma	Incremental Area [x 10^6 km^2]	Cumulative Area [x 10^7 km^2]
Present			7.78
Pliocene	5.3	3.72	7.41
Miocene	23.7	3.22	7.09
Oligiocene	36.6	9.65	6.12
Eocene	57.8	6.92	5.43
Paleocene	66.4	3.87	5.04
Late Cretaceous	84.0	5.78	4.47
Mid Cretaceous	119.0	4.50	4.02
Early Cretaceous	144.0	4.00	3.62
Late Jurassic	163.0	1.52	3.47

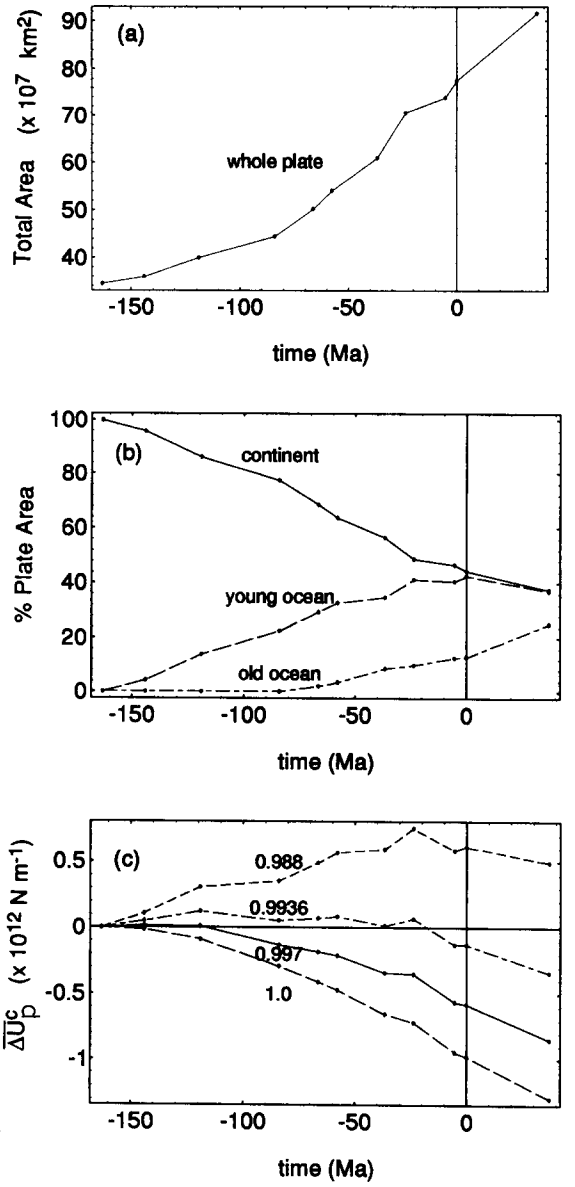

Fig. 8. (a) The cumulative area of the African plate over the past 163 Ma, and projected into the future using average Cenozoic growth rates. The primary data are listed in Table 3 and are from Royer et al. [9]. (b) The relative percentages of the principal lithospheric types for the African plate over the past 163 Ma. (c) The change in mean plate potential energy, expressed as $\Delta\overline{U}_p^c$ ($= \overline{U}_c - \overline{U}_p$, in units of $\times 10^{12}$ N m^{-1}), for the African plate. As discussed in the text, $\overline{U}_c$ was assumed to be constant during the ageing of the plate. Each figure is contoured for the range of $\overline{U}_c' = 0.988$, 0.9936, 0.997 and 1.0.

followed by an interval between the Miocene (23.7 Ma) and Pliocene (5.3 Ma) when growth slowed by a factor of four (of interest here is that extension in the East African Rift system was most active in this interval [e.g., 22]). Fig. 8a suggests that the average growth rates in the African plate have accelerated slightly throughout the last 163 Ma. Note that Fig. 8 also shows the projected changes over the next 37 Ma assuming that the Cenozoic growth rate (averaged over the last 84 Ma) is maintained.

The relative percentage of the principal lithospheric types in the African plate have varied significantly over the last 163 Ma, as shown in Fig. 8b. The percentage of continent has decreased systematically to about 46%. The proportion of young oceanic lithosphere increased rapidly between the Jurassic (163 Ma) and the Miocene (23.7 Ma), when it stabilized at about 40%. Since the Late Cretaceous (84 Ma) the percentage of old oceanic lithosphere has grown to about 14%. The projected growth rates show

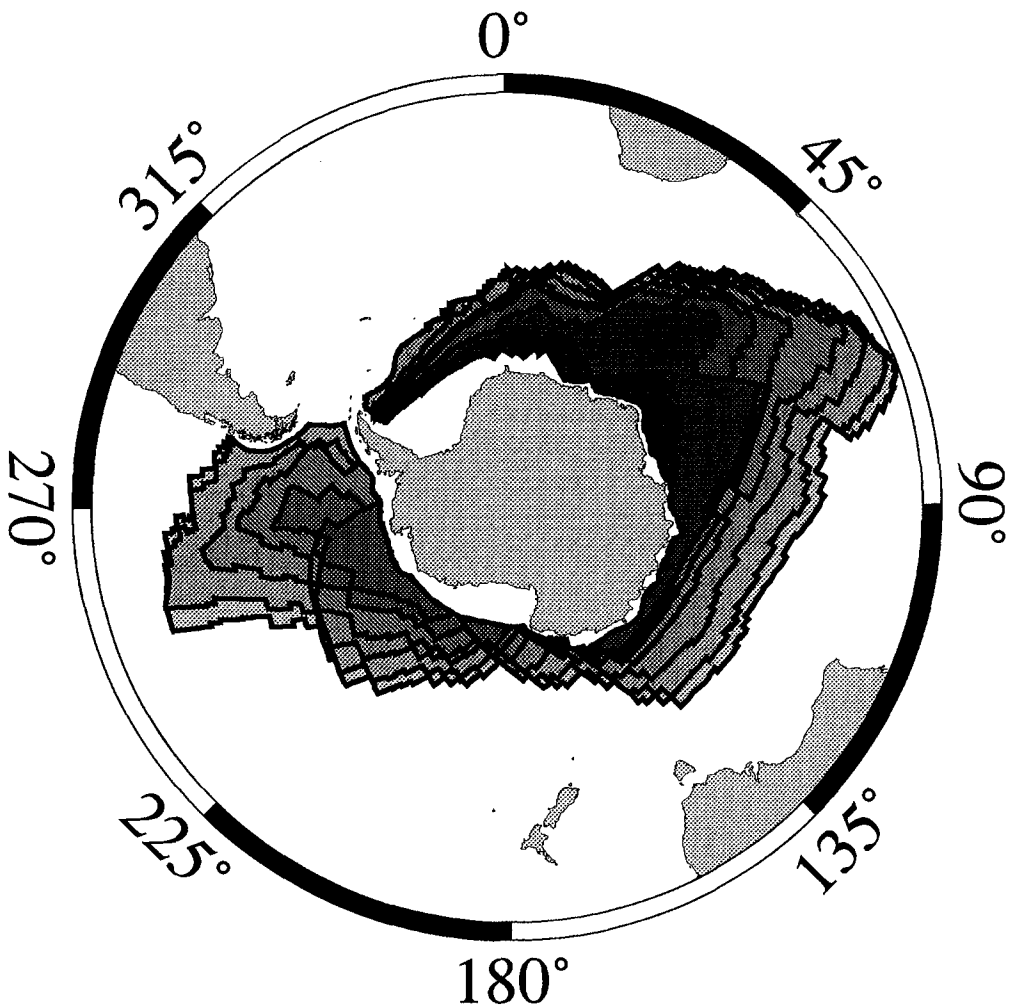

Fig. 9. The area of the Antarctic plate over the last 163 Ma. Shaded areas correspond to the area added to the plate during the Pliocene (5.3 Ma), Miocene (23.7 Ma), Oligiocene (36.6 Ma), Eocene (57.8 Ma), Paleocene (66.4 Ma), Late Cretaceous (84 Ma), mid-Cretaceous (119 Ma), Early Cretaceous (144 Ma) and late Jurassic (163 Ma) respectively (see Table 4).

the relative proportion of old ocean lithosphere will increase at the expense of both the continental lithosphere and the young ocean lithosphere over the next 37 Ma.

As discussed above, temporal variations in the relative percentages of young and old oceanic lithosphere may have a profound effect on the mean potential energy of the plate. The variation in $\overline{U}_p$ with time for the African plate is shown in Fig. 8c, for a range of $\overline{U}_c'$. For $\overline{U}_c' = 0.997$, the calculated decline in the mean plate potential energy over the last 163 Ma is $\Delta\overline{U}_p' = -0.6 \times 10^{12}$ N m^{-1}. This corresponds to an increase in the magnitude of the mean extensional stress difference $(\overline{\sigma_{zz}} - \overline{\sigma_{xx}})$ within the continents of about 5 MPa over this time period. Assuming continuation of the average Cenozoic growth rates, the projected decline in $\Delta\overline{U}_p^c$ is a further -0.25×10^{12} over the next 37 Ma.

The contrasting effects of *plate growth* and *plate ageing* on the evolving potential energy distribution within the African plate are highlighted by Fig. 8. During the rapid growth phase from the Oligiocene to Miocene the excess potential energy due to production of young ocean lithosphere counteracted the effects of ageing of the existing ocean lithosphere. Consequently, there was little net change in $\overline{U}_p$ during this period. In contrast, during the Miocene to Pliocene interval the rate of plate growth slowed by a factor of four, and the evolving potential energy distribution was dominated by plate ageing, with a relatively minor contribution through production of new ocean lithosphere. The net effect was a dramatic decline in $\overline{U}_p$ which, for $\overline{U}_c' = 0.997$, was $\Delta\overline{U}_p^c = -0.25 \times 10^{12}$ N m^{-1} over 18.4 Ma.

Fig. 8c shows that a column of the African continental lithospheric with a potential energy equal to the mean potential energy of the African continental lithosphere (i.e., a column supporting surface elevation of about 500 m) may be expected to witness extension in the ambient state provided $\overline{U}_c' > 0.993$. The predicted mean extensional stress differences are small for all reasonable values of $\overline{U}_c'$, attaining $\overline{\sigma_{zz}} - \overline{\sigma_{xx}} = 5$ and 8 MPa for $\overline{U}_c' = 0.997$ and 1.0 respectively. Such results only apply directly to those parts of the continent where the local potential energy is equal

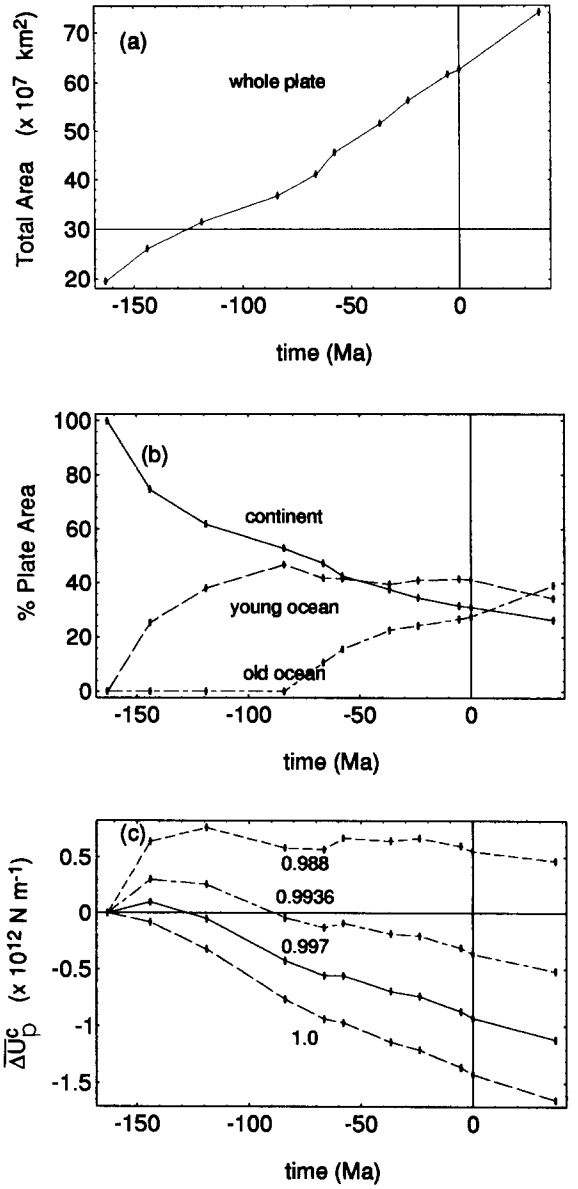

Fig. 10. (a) The cumulative area of the Antarctic plate over the past 163 Ma, and projected into the future using average Cenozoic growth rates. The primary data are listed in Table 4 and are from Royer et al. [9]. (b) The relative percentages of the principal lithospheric types for the Antarctic plate over the past 163 Ma. (c) The change in mean plate potential energy, expressed as $\Delta\overline{U}_p^c$ ($= \overline{U}_c - \overline{U}_p$, in units of $\times 10^{12}$ N m^{-1}), for the Antarctic plate. As discussed in the text, $\overline{U}_c$ was assumed to be constant during the ageing of the plate. Each figure is contoured for the range of $\overline{U}_c' = 0.988$, 0.9936, 0.997 and 1.0.

to the plate mean, and those parts of the continent with greater potential energy will witness correspondingly greater extensional stress differences. A rough estimate of the magnitude of the variations in the potential energy within the African continent is provided by the estimate (admittedly poorly constrained) that potential energy varies with topography as about 1.3×10^{12} N m^{-1} km^{-1} [21]. In the East African dome, where the average elevation approaches 2 km, the excess potential energy over the plate mean is therefore about 2.5×10^{12} N m^{-1}, corresponding to a mean extensional stress difference of about 20 MPa.

The continental lithosphere currently forms about 46% of the surface area of the African plate (Fig. 8b). The plate growth averaged over the 163 Ma gives a normalized spreading velocity of about $v' = 0.003$ Ma^{-1} (Fig. 3). For $v' = 0.003$ Ma^{-1} and $\overline{U}_c' = 0.997$, the circular plate model predicts $\Delta\overline{U}_p^c = -0.68 \times 10^{12}$ N m^{-1} over 163 Ma (Fig. 4), which compares very favourably with the more detailed estimate derived from analysis of the seafloor spreading data presented above.

4.2. The Antarctic plate

The fact that the Antarctic plate is almost completely surrounded by mid-ocean ridges with only a very small length of convergent margin in the Antarctic Peninsula sector suggests that, of all the large modern-day plates, it is most likely to *approximate* the ambient state. The growth history for the Antarctic plate over the last 163 Ma is shown in Figs. 9 and 10a, and is summarised in Table 4.

In comparison with the African plate, the somewhat smaller continental area of Antarctica, combined with a growth history which was approximately linear in time over the last 163 Ma (Fig. 10a), has resulted in a much higher proportion of old ocean to continent in the present-day Antarctic plate. As a result the time-integrated mean potential energy changes are significantly larger than calculated for the African plate. Fig. 10c shows that for $\overline{U}_c' = 0.997$ the change in mean plate potential energy $\Delta\overline{U}_p^c$ is estimated at -0.94×10^{12} N m^{-1}, corresponding to an increase in $\overline{\sigma_{zz}} - \overline{\sigma_{xx}}$ of about 7.5 MPa for a 125 km thick lithosphere.

Table 4
Area of the Antarctic plate

Age	Ma	Incremental Area [x 10^6 km^2]	Cumulative Area [x 10^7 km^2]
Present			6.26
Pliocene	5.3	0.99	6.16
Miocene	23.7	5.30	5.63
Oligiocene	36.6	4.75	5.15
Eocene	57.8	6.02	4.55
Paleocene	66.4	4.49	4.10
Late Cretaceous	84.0	4.34	3.67
Mid Cretaceous	119.0	5.27	3.14
Early Cretaceous	144.0	5.40	2.60
Late Jurassic	163.0	6.58	1.95

5. Discussion

The recognition that the growth and ageing of individual plates through seafloor spreading may significantly alter the mean plate potential energy should provide important insights into the evolution of intraplate stress fields. Assuming a continental potential-energy distribution consistent with observed geoid anomalies across continental margins we have shown that the likely net changes in $\overline{U}_p$ range up to about -1.0×10^{12} over 200 Ma (and could be significantly greater if we have underestimated the mean potential energy of the continental lithosphere). In the absence of tractions imposed at the plate boundaries or along the base of the lithosphere (i.e., in the ambient state) such changes may be expected to create significant deviatoric tension within continents in ageing plates. The magnitude of the stresses will depend on the potential energy of the local lithospheric column, as well as on the distribution of potential energy and mechanical properties [6,7] across the plate. In the ambient state the mean stress difference $(\overline{\sigma_{zz}} - \overline{\sigma_{xx}})$ increments contributed by $\Delta\overline{U}_p^c$ and are estimated to amount to up to 8 MPa averaged over the thickness of the lithospheric column. These predictions, which are

based on a very simple circular plate model, are in close agreement with estimates based on the detailed assessment of the seafloor growth history in the Antarctic and African plates.

In order to understand the role of this process in the mechanics of an ageing plate it is necessary to assess the strength of the continental lithosphere. Notions about the absolute strength of the lithosphere and the way in which such strength is distributed with depth have provided a long-standing source of entertainment (and frustration) amongst the geodynamics community. Laboratory-based strength estimates predict very heterogeneous strength distributions, with discrete strength maxima associated with compositional and rheological stratification within the lithosphere [23]. The strength of such a lithosphere is clearly dependent on both the lithological constitution and the thermal regime, both of which are known to vary widely. On the basis of such laboratory estimates a number of workers [e.g., 2,24] have suggested that the extensional strength of the lithosphere at the limit of geologically significant strain rates is of the order or $3\text{–}4 \times 10^{12}$ N m^{-1}. More recently, Kusznir [25] has argued that extensional strength may be considerably reduced, possibly to as little as 2×10^{12} N m^{-1}, due to the viscoelastic amplification of stresses in the lithosphere. While such estimates are highly uncertain they are of interest here in as much as the predicted changes in $\Delta\overline{U}_p^c$ represent a significant fraction (up to 25–50%) of these strength estimates. The implication is that providing the continental stress field feels the changes in $\Delta\overline{U}_p^c$ that accompany plate ageing, as we suggest it should in the ambient state, then the evolving density structure of an ageing plate engenders the very real possibility of extensional failure and fragmentation. In the modern Earth the only plates largely surrounded by mid-ocean ridge systems, and therefore likely to approximate the ambient stress state, are the African and Antarctic plates, and both show evidence of active, or recently active, continental extension. While other processes such as the active involvement of mantle plumes may have contributed to the location and initiation of such extension, we suggest that the conditions for such extension have been significantly aided by the ageing of these plates, as their peripheral ocean ridges spread outwards, and $\overline{U}_p$ declines.

An important question concerning the interpretation of the ambient stress state is whether the continental lithosphere will see the effects of the plate-scale potential-energy distribution as proposed here. A number of previous workers have briefly touched on the question of the potential-energy variation across lithospheric plates [e.g., 2,7]. Houseman and England [2] acknowledged the "potential energy contrast between continental lithosphere and old ocean basins" but argued "that in general this does not result in (continental) extension, presumably because the oceanic lithosphere acts rigidly to transmit the stresses arising from the midocean ridges". This argument assumes implicitly that the ocean ridge system defines a *tectonic reference* state and in the ambient state must therefore be in near potential-energy balance with the mean plate potential energy (see Coblentz et al. [11] for a discussion of the concept of a tectonic reference state). This notion is founded on the belief that the mid-ocean ridges are sufficiently weak that they could not sustain substantial extensional stresses (but see Fleitout and Froidevaux [7] for an alternative view). While acknowledging that mid-ocean ridges must be very weak, we note that the active extension, which is manifestly occurring at the ridges (and elsewhere), requires not only an excess potential energy (i.e., a driving force) but also the kinematic requirement that accommodates the extension (i.e., a displacement). The extension along the ridges bounding most plates, and particularly the African and Antarctic plates, is not currently being accommodated by the internal compressional deformation of these plates but rather by global plate kinematic constraints. This implies that the parts of the plate with potential energy less than the plate mean (such as the old oceanic lithosphere) are sufficiently strong to withstand the compressional forces imposed by the ridges and the other parts of the plates with excess potential energy. We note that the lack of accommodating displacements internally within these plates allows (but does not require) ridges to be able to withstand significant excess poten-

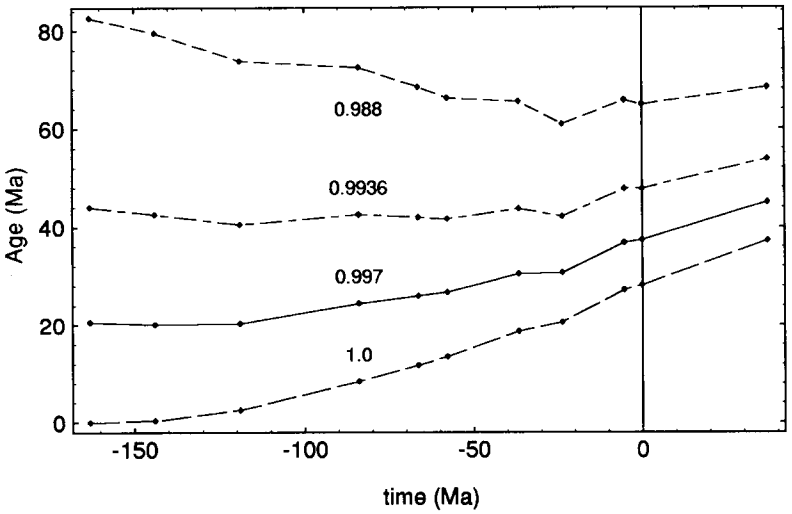

Fig. 11. Age of ocean lithosphere with potential energy corresponding to the mean plate potential energy (i.e., $U_l = \overline{U}_p$) plotted as a function of age for the African plate using the plate growth data summarized in Fig. 8. Contours show the range of $\overline{U}'_c = 0.988$, 0.9936, 0.997 and 1.0.

tial energy independently of their inherent strength.

It may be postulated that one plausible test of the notions developed in this paper concerns the nature of the stress fields in the ridge systems and ocean basins surrounding supposedly near-ambient plates. Fig. 11 shows how the age of the ocean lithosphere with the potential energy corresponding to mean plate potential energy (i.e., $U_l = \overline{U}_p$) evolves with time for the African plate. Assuming that the stress distribution is not greatly affected by radial variations in mechanical properties of the lithosphere, in the ambient state ocean lithosphere of this critical age will experience no deviatoric stress while younger lithosphere should experience deviatoric tension and older lithosphere should experience deviatoric compression. For $\overline{U}'_c = 0.977$, we predict that this critical age increases from about 20 to 38 Ma over the 163 Ma history since the late Jurassic. One implication of this is that, in the modern African plate, the compression witnessed by old ocean lithosphere ($t > 84$ Ma) is only about half the so-called 'ridge push' force which is traditionally formulated in terms of the difference between the potential energy of the mid-ocean ridges and old ocean lithosphere. This critical age range is consistent with the global oceanic seismic dataset which suggests the transition from tension to compression in ocean lithosphere typically occurs in the lithospheric age range 20–40 Ma [e.g., 26]. However, since the global dataset is strongly biased by events in the Indo-Australian plate, where the intraplate stress field is far from ambient, a more detailed analysis from the African and Antarctic ocean basins is required to test the ideas presented here. Unfortunately, the generally low levels of stress in the ocean basins in these plates predicted by the analysis presented in this paper suggests levels of ocean-basin seismicity so low as to preclude a detailed evaluation of their stress field, a prediction which is in accord with the low levels of recorded seismicity within the ocean lithosphere of the African and, particularly, the Antarctic plate.

Acknowledgements

This work was initiated through funds made available by the Australian Petroleum Cooperative Research Centre as part of a study of the factors controlling the intraplate stress field along the northwest shelf of Australia. We are greatly

indebted to our colleagues working on this project, Richard Hillis and Shaohua Zhou, for their encouragement and suggestions. Randy Richardson is thanked for many illuminating discussions concerning intraplate stress fields and the African plate problem. Kurt Stuwe and two anonyous 'EPSL' reviewers are thanked for comments on an early version of the manuscript.

References

[1] S.T. Crough, Rifts and swells: Geophysical constraints on causality, Tectonophysics 94, 23–37, 1983.
[2] G. Houseman and P. England, A dynamical model of lithosphere extension and sedimentary basin formation, J. Geophys. Res. 91, 719–729, 1986.
[3] N. Pavoni, Rifting of Africa and pattern of mantle convection beneath the African plate, Tectonophysics 215, 35–53, 1992.
[4] F.C. Frank, Plate tectonics, the analogy with glacier flow and isostasy, flow and fracture of rocks, AGU Geophys. Monogr. 16, 285–292, 1972.
[5] E.V. Artyushkov, Stresses in the lithosphere caused by crustal thickness inhomogeneities, J. Geophys. Res. 78, 7675–7708, 1973.
[6] L. Fleitout and C. Froidevaux, Tectonics and topography for a lithosphere containing density heterogeneities, Tectonics 1, 21–56, 1982.
[7] L. Fleitout and C. Froidevaux, Tectonic stresses in the lithosphere, Tectonics 2, 315–324, 1983.
[8] F.A. Dahlen, Isostasy and the ambient state of stress in the oceanic lithosphere, J. Geophys. Res. 86, 7801–7807, 1981.
[9] J.-Y. Royer, R.D. Mueller, L.M. Gahagan, L.A. Lawver, C.L. Mayes, D. Nuernberg and J.G. Sclater, A global isochron chart, Univ. Texas Inst. Geophys. Tech. Rep. 117, 38 pp., 1992.
[10] D.L. Turcotte and G. Schubert, Geodynamics: Applications of Continuum Physics to Geological Problems, 450 pp., Wiley, New York, 1982.
[11] D. Coblentz, R. Richardson and M. Sandiford, On the gravitational potential of the Earth's lithosphere, Tectonics, in press, 1994.
[12] D.L. Turcotte and D.L. McAdoo, Geoid anomalies and the thickness of the lithosphere, J. Geophys. Res. 84, 2381–2387, 1979.
[13] W.F. Haxby and D.L. Turcotte, On isostatic geoid anomalies, J. Geophys. Res. 83, 5473–5478, 1978.
[14] B. Parsons and F.M. Richter, A relation between driving force and geoid anomaly associated with the mid-ocean ridges, Earth Planet. Sci. Lett. 51, 445–450, 1980.
[15] D.T. Sandwell and G. Schubert, Geoid height versus age for symmetric spreading ridges, J. Geophys. Res. 85, 7235–7241, 1980.
[16] D.W. Forsyth, Geophysical constraints on mantle flow and melt generation beneath ocean ridges, AGU Geophys. Monogr. 71, 1–65, 1992.
[17] S.T. Crough, Geoid anomalies across fracture zones and the thickness of the lithosphere, Earth Planet. Sci. Lett. 44, 224–230, 1979.
[18] P. Wessel and W.F. Haxby, Geoid anomalies at fracture zones and thermal models for the oceanic lithosphere, Geophys. Res. Lett. 16, 827–830, 1989.
[19] L.J. Sonder, P.C. England, B.P. Wernicke and R.L. Christiansen, A physical model for Cenozoic extension of western North America, in: Continental Extensional Tectonics, M.P. Coward, J.F. Dewey and P.L. Hancock, eds., Geol. Soc. London Spec. Publ. 28, 187–201, 1987.
[20] S. Zhou and M. Sandiford, On the stability of isostatically compensated mountain belts, J. Geophys. Res. 97, 14207–14221, 1992.
[21] C. Froidevaux and B.L. Isacks, The mechanical state of the lithosphere in the Altiplano–Puna segment of the Andes, Earth Planet. Sci. Lett. 71, 305–314, 1984.
[22] W. Bosworth, M.R. Strecker and P.M. Blisniuk, Integration of East African and present-day stress data: Implication for continental stress field dynamics, J. Geophys. Res. 97, 11851–11865, 1992.
[23] W.F. Brace and D.L. Kholstedt, Limits of lithospheric stress imposed by laboratory experiments, J. Geophys. Res. 85, 6248–6252, 1980.
[24] N. Kusznir and R. Park, The extensional strength of the continental lithosphere: its dependence on geothermal gradient and crustal composition and thickness, in: Continental Extensional Tectonics, M.P. Coward, J.F. Dewey and P.L. Hancock, eds., Geol. Soc. London Spec. Publ. 28, 35–52, 1987.
[25] N. Kusznir, The distribution of stress with depth in the lithosphere: thermo-rheological and geodynamic constraints, in: Tectonic Stress in the Lithosphere, R.B. Whitmarsh, M.H.P. Bott, J.D. Fairhead and N.J. Kusznir, eds., pp. 95–110, R. Soc., London, 1991.
[26] S. Stein and A. Pelayo, Seismological constraints on stress in the ocean lithosphere, in: Tectonic Stress in the Lithosphere, R.B. Whitmarsh, M.H.P. Bott, J.D. Fairhead and N.J. Kusznir, eds., pp. 53–70, R. Soc., London, 1991.
[27] D.D. Coblentz and R.M. Richardson, Constraints on continental margin dynamics from GEOSAT ERM data, AGU Fall Meet. Abstr. 73, p. 571, 1992.